Dynamics Final Project Report

Zeshui Song, Roy He, Ryan Lee

Introduction to project

In all modern cars, the suspension system helps absorb forces from bumps, steering, and acceleration/braking. The behavior of the car under these forces is called vehicle dynamics. The goal of this project is to characterize the dynamic response of the Cooper Union FSAE car's suspension. We will model the system's free oscillation following an initial displacement, and validate our model by comparing it to video tracking of the suspension spring's motion after being released from a compressed state.

Assumptions

For this model, we assume a massless suspension system where the wheel remains fixed while the chassis moves. This assumption can be made because the weight of all the suspension components, calculated by multiplying the linear density of the 0.5" steel rod by the total length (about 2.9'), using a density of steel of 0.284 lb/cubic inch, comes out to under 2 lb. The actual weight of the suspension is lower due to the rods being hollow, so 2 lb is the very upper bound of this value. The car itself weighs over 500 lb when fully loaded, therefore the mass of the suspension is less than 0.4% of the weight of the car, making their inertial effects negligible for these simulations.

Furthermore, the kinematic analysis is restricted to the upper control arm, pushrod, shock mount, and shock absorber. While the lower control arm is critical for determining vehicle behavior during driving, it does not govern the linear displacement of the shock or the vertical travel of the wheel for the specific purposes of this load simulation. Therefore, we can simplify the suspension system to a four-bar linkage system, as shown in Figure 1.
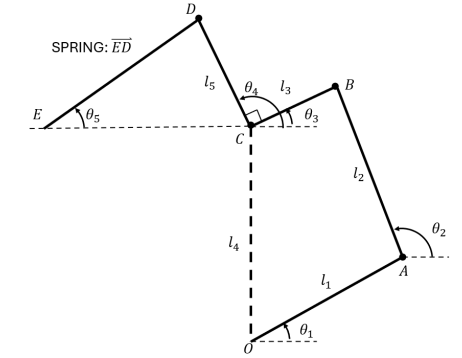

Figure 1: Four-bar linkage model of the suspension system, composed of the upper control arm (l_1), the pushrod (l_2), and the shock mount (l_3 and l_5). The chassis (l_4) serves as the fixed ground link.

Geometric Solution for Linkage Kinematics

Our objective is to determine the angles $\theta_2, \theta_3, \theta_4,$ and θ_5 given the input angle θ_1. While vector loops can be used, While vector loops can be used, we utilized a geometric approach finding the intersection of circles centered at pivots A and C, as described by Norton [1]. Referring to Figure 2, we outline the steps below.

First, we define the positions of the known pivots A and C and the vector $\vec{d}$ connecting them:

$$\vec{A} = \langle l_1 \cos\theta_1, l_1 \sin\theta_1 \rangle$$
$$\vec{C} = \langle 0, l_4 \rangle$$
$$\vec{d} = \vec{C} - \vec{A}, \quad d = \|\vec{d}\|$$

We solve for point B by viewing $\triangle ABC$ as two right triangles sharing a height h. The projection a of link l_2 onto vector $\vec{d}$ and the orthogonal height h are:

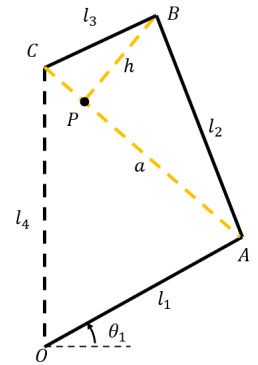$$a = \frac{l_2^2 - l_3^2 + d^2}{2d}, \quad h = \sqrt{l_2^2 - a^2}$$

Figure 2: Geometry of the linkage variables.

Point B is located by traversing distance a along the unit vector $\hat{d}$ and distance h along the perpendicular vector $\hat{d}_\perp$:

$$\vec{B} = \vec{A} + a\hat{d} + h\hat{d}_\perp \quad \text{where} \quad \hat{d}_\perp = \left\langle -\frac{d_y}{d}, \frac{d_x}{d} \right\rangle$$

With coordinates for A, B, and C known, vectors $\vec{l_2}$ and $\vec{l_3}$ are fully defined. Point D is then found using the normal vector of $\vec{l_3}$ and using the length l_5. With points D and E, we have fully defined the system and can find all the angles using trigonometry.

Suspension Load Calculations

We will determine the forces in each link using rigid-body static equilibrium, based on the assumption that the suspension is massless. As seen in Figure 3, there are 9 unknowns $(A_x, A_y, B_x, B_y, C_x, C_y, O_x, O_y, N)$ and we have the following 9 equations:

- Sum of forces and moments in the shock mount:

$$\sum F_x = F_s\cos\theta_5 + C_x - B_x = 0$$

$$\sum F_y = F_s\sin\theta_5 + C_y - B_y = 0$$

$$\sum M_C = l_5 F_s \sin(\theta_5 - \theta_4) - l_3 B_y \cos\theta_3 + L_3 B_x \sin\theta_3 = 0$$

- Sum of forces and moments in the upper control arm (l_1):

$$\sum F_x = O_x + A_x = 0$$

$$\sum F_y = O_y + A_y = 0$$

$$\sum M_O = -l_1 A_x \sin\theta_1 + l_1 A_y \cos\theta_1 = 0$$

Figure 3: FBDs of disassembled suspension components. Where N is the normal reaction force on the pushrod, and F_s is the force from the shock absorber.

- Sum of forces and moments in the pushrod (l_2):

$$\sum F_x = B_x - A_x = 0$$

$$\sum F_y = B_y - A_y + N = 0$$

$$\sum M_B = -l_2 B_x \sin\theta_2 + l_2 B_y \cos\theta_2 = 0$$

Forming a matrix from these 9 equations allows us to solve for the unknown forces in the suspension system. Particularly, we are interested in the normal reaction force N acting on the pushrod shown in Figure 4, which will be used to calculate the effective spring constant of the suspension.

Effective Spring Constant Calculation

Since the suspension geometry changes with wheel displacement, the system does not obey a linear Hooke's Law $(F = ky)$. Instead, we calculate the effective spring constant as the derivative of the vertical force (N) with respect to vertical displacement of the wheel (dN/dy). This method was based on the approach for finding the wheel rate in a moving suspension system by Milliken and Milliken [2]. Numerically solving for dN/dy yields the effective spring constant plot shown in Figure 5.
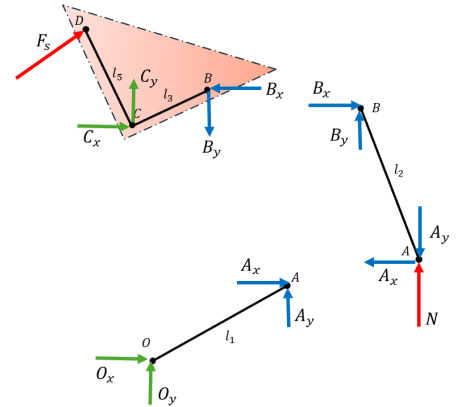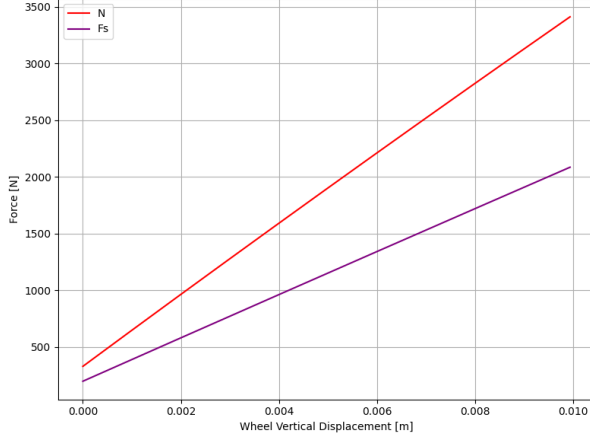
Figure 4: Normal reaction force N on the pushrod as a function of wheel displacement.
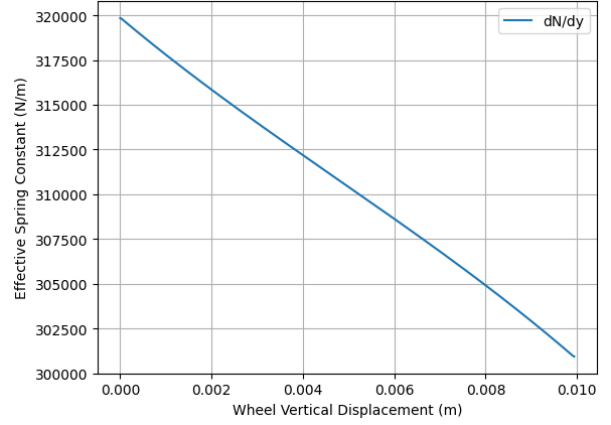

Figure 5: Effective spring constant $k_{eff} = dN/dy$ as a function of wheel displacement.

Spring Mass Simulation and Validation

Knowing the effective spring constant as a function of wheel displacement, we can simulate the free oscillation of the car chassis as a mass-spring system using the ODE:

$$m\frac{d^2y}{dt^2} + c\frac{dy}{dt} + k_{\text{eff}}(y) \cdot (y - y_{\text{eq}}) = 0$$

Determining the initial conditions $y(0) = -0.0233\,\text{m}$, $y'(0) = 0\,\text{m/s}$, and $y_{\text{eq}} = -0.0295\,\text{m}$ from video analysis of the actual suspension oscillation, we numerically solved this ODE using Python's `solve_ivp` function. The mass and damping coefficient were tuned to best fit the experimental data, resulting in $m = 1000\,\text{kg}$ and $c = 1500\,\text{Ns/m}$. The simulation models the vertical displacement of the car chassis over time, which is shown in Figure 6.
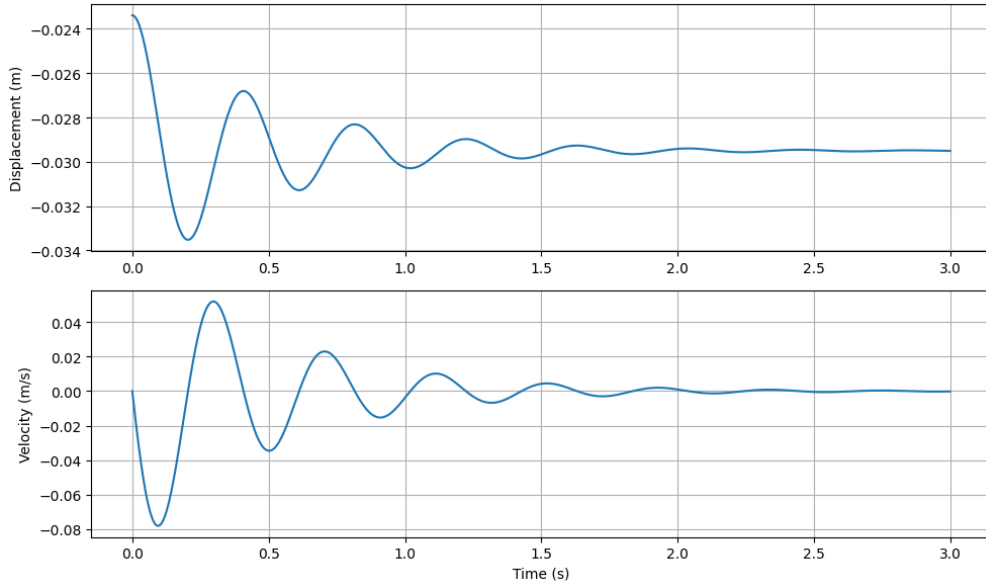

Figure 6: Simulated car chassis vertical displacement and velocity over time using the nonlinear effective spring constant.

To validate our model, the simulated car chassis displacement over time is converted to spring displacement used our kinematic linkage model to map the simulated chassis displacement $y(t)$ back to the equivalent spring displacement. This is compared to the experimental spring displacement obtained from video tracking in Figure 7. The simulation showed similar long term behavior and frequency of oscillation to the experimental data, both settling around the same equilibrium position.
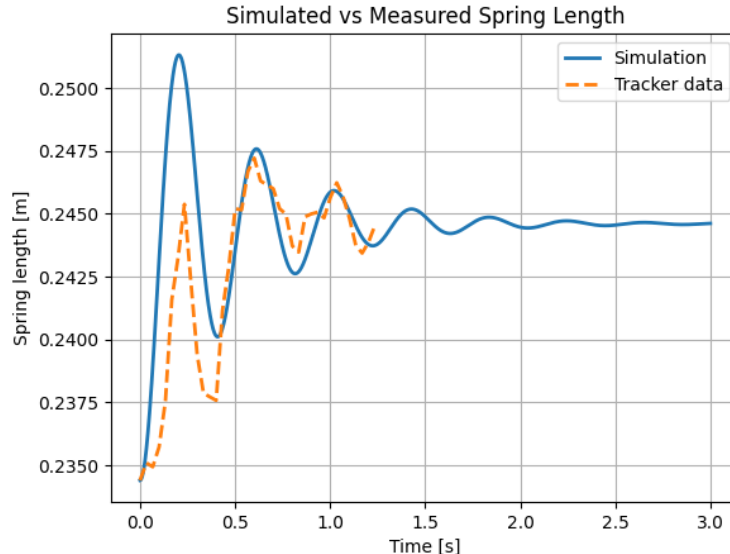

Figure 7: Comparison of simulated and experimental suspension oscillation.

Results

Based on the results of tracker and the simulation, the simulation does partially align with reality, as per Figure 7. This is because both plots have what appears to be exponential decay for the amplitude of oscillation, which would match the expected solution to the damped mass oscillator equation. However, there is a constant friction in the real system, as well as the real drag in the shock increasing with velocity of the system, so the oscillations at higher amplitudes which correspond with higher suspension velocity get damped faster.

Additionally, the simulated mass of 1000 kg is significantly higher than the actual mass of the car, which is around 226.796 kg. Since the natural frequency is governed by $\omega = \sqrt{k/m}$, and the mass was adjusted to match the experimental oscillation frequency. This discrepancy indicates that our derived effective spring constant overestimates the real suspension stiffness by about a factor of four. This could be due to the geometrical simplifications made in the model, where we neglected the internal reaction forces from the other suspension components such as the lower control arm, wheel hub, and tires. Additionally, our model placed the pushrod joint at the very end of the upper control arm, whereas in reality it is located slightly inboard. This change in geometry would reduce the mechanical advantage of the pushrod, leading to a lower effective spring constant.

References

[1] R. L. Norton, *Design of Machinery: An Introduction to the Synthesis and Analysis of Mechanisms and Machines*, 2nd ed., New York, NY: McGraw-Hill, 1999, pp. 152–153.

[2] W. F. Milliken and D. L. Milliken, *Race Car Vehicle Dynamics*, Warrendale, PA, USA: SAE International, 1995.